THE ASTROPHYSICAL JOURNAL, 397:214–224, 1992 September 20

NEUTRAL WINDS FROM PROTOSTARS

CARLO GIOVANARDI
Osservatorio Astrofisico di Arcetri and CAISMI-CNR, Largo E. Fermi 5, I-50125 Firenze, Italy

SUSANA LIZANO
Instituto de Astronomia UNAM, Ap.do Postal 70-264, 04510 Ciudad Universitaria, Mexico

ANTONELLA NATTA
Osservatorio Astrofisico di Arcetri, Largo E. Fermi 5, I-50125 Firenze, Italy

NEAL J. EVANS II
University of Texas, Astronomy Department, Austin, TX 78712

AND

CARL HEILES
University of California, Astronomy Department, Berkeley, CA 94720
Received 1991 November 19; accepted 1992 March 27

ABSTRACT

We present Arecibo 21 cm line observations of neutral winds associated with young stellar objects. We confirm the detection of fast neutral winds in HH 7–11 and in L1551. These two winds have been coarsely mapped along the CO outflow direction. For the case of HH 7–11, we find that the maximum velocity declines from 170 km s^{-1} at the center (SVS 13), to $\sim$135 km s^{-1} at a position displaced half a beam away from the center. This finding is consistent with the idea that the neutral wind is partially resolved by our observations and decelerates away from the source SVS 13. In contrast, the extent of the outflow in the case of L1551 is well resolved by the Arecibo beam and we present a map of the high-velocity H I gas along the red CO lobe. The H I observations of HH 7–11 and L1551 support the picture in which the CO outflow is driven by a fast neutral stellar wind that conserves momentum and drives the observed high-velocity molecular outflows. From the observations, the maximum mass-loss rate (assuming a constant velocity wind) and maximum velocity for HH 7–11 are $\dot{M} = 8.8 \times 10^{-6}$ $M_\odot$ yr^{-1} and $v \sim 170$ km s^{-1}. For L1551 they are $\dot{M} = 6 \times 10^{-6}$ $M_\odot$ yr^{-1} and $v \sim 260$ km s^{-1}. The high-velocity H I in L1551 extends up to the end of the CO lobe which means that a substantial fraction of the momentum and energy of the wind must be deposited, possibly through a shock, into the ambient cloud. We find that the high-velocity H I along the red lobe has the characteristic triangular profiles indicative of deceleration. For this object we present a simple model of the process of mass entrainment in the atomic wind which reproduces the intensity and shape of the observed line profiles.

High-velocity H I gas was searched and not detected in five more objects: RNO 43, R Mon, NGC 2264, B335, FU Ori. For these objects we obtain upper limits on the atomic high-velocity gas which are not stringent. Therefore, even if no high-velocity H I was detected, the observed molecular outflows could still be driven by massive neutral winds. Finally, the upper limit on the atomic mass in the case of FU Ori sets a limit on the mass-loss rate during the active phase which initiated with the outburst in 1937. Again, this is not a stringent limit because it is still an order of magnitude larger than the mass-loss rates required by current models of FU Ori objects.

Subject headings: radio lines: atomic — stars: mass loss — stars: pre–main-sequence

1. INTRODUCTION

Considerable evidence supports the view that star formation is accompanied by a simultaneous outflow of matter. Since this simultaneity is conceivable only in a nonspherical geometry, a picture has formed of star formation mainly through disk accretion, with the outflow occurring in the polar direction not blocked by the infalling gas. In this picture, the outflow is an important part of the star formation process and quantitative measurements of the rate of mass outflow ($\dot{M}$) are valuable constraints on models of star formation.

Fast winds ($v_w \sim$ 100–300 km s^{-1}) from T Tauri stars have been known for some time based on P Cygni profiles seen in various lines at visual wavelengths (e.g., Appenzeller & Mundt 1990). However, quantitative determination of $\dot{M}$ from these lines is difficult (e.g., De Campli 1981). Near-IR hydrogen recombination lines have also been detected which can be used to constrain $\dot{M}$ (e.g., Giovanardi et al. 1990). On the other side, the youngest objects are still deeply embedded in molecular clouds, making the optical lines and the near-IR lines generally undetectable. Nonetheless, abundant evidence for an outflow has been found in these embedded objects, namely optical jets, Herbig-Haro objects (e.g., Raga 1989), H_2O maser emission, broad wings on CO profiles, and extended features revealed by near-IR images (e.g., Terebey et al. 1991). Quantitative measurements of v_w and $\dot{M}$ are not easily obtained. Radio continuum observations of ionized winds imply a mass-loss rate too small (factors of 100) to drive the high-velocity CO lobes (Rodríguez & Cantó 1983; Snell et al. 1985; Strom et al. 1986). Also the mass-loss rates obtained from infrared hydrogen lines are considerably lower (factors of 10–100) than those derived

from CO (Evans et al. 1987). Finally, there is again a discrepancy between the mass-loss rates derived from optical jets and those from the outflows (Mundt, Brugel, & Bührke 1987).

The discrepancy between these different tracers of mass loss can be resolved if the stellar winds are primarily neutral, and calculations of the ionization structure and line emission from cool winds ($T_w \sim 6000$–8000 K) confirm this suggestion (Natta et al. 1988; Natta, Giovanardi, & Palla 1988). On the other hand, the wind mass-loss rates derived from CO [$\dot{M}$(CO)] rely on the assumption that the molecular gas has been swept up by a stellar wind, conserving only the momentum of the wind (see, e.g., Levreault 1988a). This assumption is supported by the finding of a shell structure in the molecular outflow in L1551 (e.g., Moriarty-Schieven & Snell 1988) and B335 (Hirano et al. 1988). Simple models of momentum conserving winds can explain many of the observed properties of the CO outflows (Shu et al. 1991). Momentum conservation implies that

$$\dot{M}(\mathrm{CO}) = \frac{M(\mathrm{CO})}{\tau(\mathrm{CO})}\frac{v_{\mathrm{CO}}}{v_w}.$$

This method would overestimate $\dot{M}$ by a factor v_w/v_{CO} if the whole shock energy is converted to motion of the molecular gas, rather than being mostly radiated away (Dyson 1984; Kwok & Volk 1985). Models of massive stellar winds capable of driving the CO outflows have been proposed (Shu et al. 1987), but other models have been devised in which the high-velocity CO is accelerated in a shell by a toroidal magnetic field, not by a stellar wind (Shibata & Uchida (1985), and models in which the high-velocity CO is coming from a disk wind (Pudritz & Norman 1983) not having a shell structure.

Even if the basis of the CO method is correct, $\dot{M}$(CO) is uncertain within a factor of 10 because of the uncertainties in deriving M(CO), τ(CO) and v_{CO} from the observations, e.g., the uncertainty in the CO/H_2 conversion factor. Moreover, v_w is rarely known for embedded objects (Levreault 1988a; Cabrit & Bertout 1990). All these uncertainties enhance the importance of independent measurements of $\dot{M}$ and of consistency checks for the basic picture.

Natta & Giovanardi (1990) have used Na I lines in combination with Brγ, to derive $\dot{M}$ and the wind temperature T_w from five T Tauri stars. They found low wind temperatures, $T_w \sim 6000$ K, and $\dot{M}$ rates in excellent agreement with $\dot{M}$(CO) for the three stars where $\dot{M}$(CO) is available. Unfortunately, this test requires sufficiently low extinction to see Na I lines near 5900 Å, but enough surrounding molecular material to produce CO lobes.

Another approach is suggested by the conclusion that the winds are neutral; in this case, the wind may be directly detectable in the 21 cm line of H I, but the predicted emission is weak and easily confused by the ubiquitous Galactic H I. After the seminal work of Bally & Stark (1983), Lizano et al. (1988, hereafter Paper I) were able to detect an H I wing in the direction of the driving source of the HH 7–11 outflow, and a marginal detection toward L1551 IRS 5. Recently, Ruiz, Alonso, & Mirabel (1991) have detected a neutral wind in T Tau. Finally, Russell et al. (1991) detected an atomic wind associated with the H II region DR21 which is three orders of magnitude more massive than the atomic winds of the previous three objects.

Since the direct observation of the neutral wind allows a straightforward determination of its mass, as well as v_w, even in very deeply embedded objects, we have made further observations of the 21 cm line towards HH 7–11 and L1551 IRS 5. In addition, other low luminosity, young, nearby objects were selected because they had observed molecular outflows or other possible indication of massive winds. Of these sources we could observe RNO 43, FU Ori, R Mon, NGC 2264, and B335, but we obtained only upper limits to the mass of H I in the wind.

2. OBSERVATIONS

The observations took place at the Arecibo[1] 1000 ft radiotelescope in two separate runs during winter 1988–89 and 1989–90, respectively. All the spectra were acquired using the 1415 MHz dual circularly polarized line feed connected to helium-cooled GaAs FET receivers. The beam size at low zenith angle was about 3.2, with an average value of 3.5 (FWHM). The pointing was routinely checked and found accurate to about 30″ rms. The calibration in antenna temperature (T_A) was obtained using the most recent laboratory checks of the receiver noise diodes. The stability of the diodes was also routinely checked during the runs and found to be constant within 5%, rms. During the observations the feed was tuned at 1418 MHz; in this configuration the overall forward gain at 1420 MHz was found to be 7.5 K Jy^{-1}. The average cold sky system temperature (T_{sys}) near zenith was about 45 K.

Two different observing methods were adopted. The actual search for neutral winds was performed by beam switching (B.S.) between the source (ON) position and two different reference (OFF) positions symmetrically displaced from the ON. The OFF's were typically displaced by 10′ from the ON position, in directions perpendicular to the outflow axis. If the source was mapped, the same OFF positions were used for the different ON's. In three cases, that is for HH 7–11, L1551, and NGC 2264, we also observed the field around the source, with shorter integration time, to map the general behavior of the Galactic H I in these areas. These lower sensitivity spectra were acquired with a frequency switching (F.S.) "within the band" method. In both cases of beam and frequency switching a 10 MHz bandwidth, from each polarization, was fed into a bank of 1024 channels of the 2048 channel digital correlator. The resulting spectral resolution, after Hanning smoothing, is 3.9 km s^{-1}; the total spectral coverage is 2110 km s^{-1} in B.S. and half of this in F.S. after folding.

The F.S. data were acquired mainly to check the amplitude at high velocities and the spatial variation of the H I Galactic line in some relevant areas. The integration time was limited to 2 minutes per position, which resulted into an rms noise of $\sim$0.07 K at a resolution of 3.9 km s^{-1}, this is much noisier than the final B.S. spectra. We obtained one-dimensional maps along the outflow direction (position angle 40°) and perpendicular to it in L1551; we used a stepsize of 3′ and observed 14 points on each side of IRS 5. A similar procedure was used in the case of HH 7–11 and NGC 2264 but mapping only 10 points on each side of the central position in an east-west direction. We will not discuss here these data except for noting that some structures, such as the cloud system which chops up the blue side of the L1551 B.S. spectra, exhibit notable variations (0.05 K) on a few arcmin scale, and that the intrinsic width of the H I pedestal, even away from the wind region and

[1] The Arecibo Observatory is part of the National Astronomy and Ionosphere Center which is operated by Cornell University under contract with the National Science Foundation.

even in the anticenter region, appears to extend to rather high velocities, e.g., up to $V_{LSR} = 90$ km s^{-1} on the red (undisturbed) side in the L1551 area ($l_{II} = 178.9$, $b_{II} = -20.0$).

The B.S. data were always acquired using two different reference positions in an OFF1-ON-ON-OFF2 pattern. To improve the baseline quality the integration times on each position were limited to 1 minute and, for the duration of a single pattern, the gain settings of the electronics and the frequency of the local oscillators were not altered. The pattern was then repeated to accumulate a suitable integration time. The B.S. spectra were obtained with the usual procedure (ON-OFF)/OFF and multiplying by the average T_{sys} in the OFF position. For each pattern three spectra were computed: ON versus OFF1, ON versus OFF2, and OFF1 versus OFF2. The last spectrum allowed us to check the degree of cancellation between the OFF's of any winglike feature which could stem from gradients in the high-velocity "background" emission. In case the cancellation was not deemed adequate (<0.01 K), another pair of OFF's, typically displaced a few arcmin from the previous one, was chosen. Our beam switching observations are summarized in Table 1. The overall quality of the spectra can be appreciated in Figure 1 which depicts the final spectrum for the central position in HH 7−11. Apart from some degrading at the very edges ($V_{LSR} < -900$ km s^{-1} and $V_{LSR} > 1000$ km s^{-1}) any baseline rippling appears to be well contained within the noise level. Notably, as in Paper I, the spectra were only Hanning smoothed once and only linear baselines have been subtracted. The accuracy of the final T_A calibration is around 10%, including zenith angle and frequency corrections. This does not apply, however, to the low (absolute) velocity range of the B.S. spectra, i.e., in the line core. Here, in fact, also the reference position has T_A which amounts to a sensible fraction (up to 100 K) of T_{sys}. This leads to underestimate T_A in the core of the line by about a factor of 2.

Since we were looking for extremely weak, broad features adjacent to a relatively narrow and very intense one (i.e., the Galactic H I line core), we checked the possibility that they could be due to some spectral spill over in the correlator, or more generally in the backend chain. In fact the contrast between the line core and our detected wings is around 10^4 and doubts arise about the possibility of some contamination between the spectral channels. Such a possibility was tested by

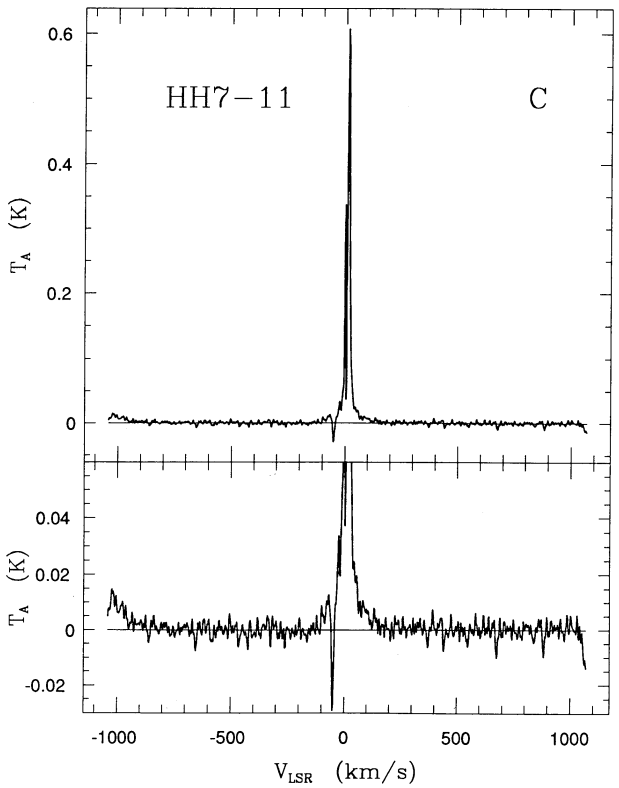

FIG. 1.—In the upper panel we present an H I spectrum taken at arecibo of HH 7−11 centered on SVS 13. The lower panel shows the same spectrum but with a blown-up vertical scale. Only a linear baseline has been subtracted. Except at the velocity extremes, any deviation of the baseline from horizontal is contained within the noise.

TABLE 1

BEAM SWITCHING OBSERVATIONS

NAME	POSITION	EQUATORIAL COORDINATES (1950) R.A.	Decl.	V_{LSR} (km s^{-1})	OFF PAIRS	ON INTEGRATION (minutes)
HH 7−11	C	03^{h}25^{m}58^s.2	31°05′46″	8.2	2	226
	NW1	03 25 54.2	31 07 00	...	2	250
	NW2	03 25 52.5	31 08 30	...	2	218
	NW3	03 25 50.0	31 10 30	...	2	112
	SE1	03 26 04.9	31 05 06	...	2	134
L1551	C	04 28 40.0	18 01 42	7.0	2	225
	NE1	04 28 52.2	18 02 48	...	2	134
	NE2	04 29 00.0	18 05 11	...	2	174
	NE3	04 29 07.5	18 07 36	...	2	124
RNO 43	N	05 29 38.5	12 55 15	10.0	1	56
	S	05 29 36.0	12 50 30	...	1	58
FU Ori	C	05 42 38.2	09 03 02	12.0	3	282
R Mon	C	06 36 25.9	08 46 57	9.4	2	152
NGC 2264	C	06 38 25.0	09 31 12	10.0	1	132
B335	W	19 34 24.0	07 27 30	8.5	2	142
	E	19 34 49.0	07 27 30	...	2	184

simulating numerically the response of the digital correlator in similar conditions and by directly injecting narrow band, strong signals into the IF amplifiers. In no case could we generate spurious wings of the required intensity and width. In fact, both the simulated and the measured spectra developed, in such conditions, rather strong high-frequency ringings with a two channel period (which are then completely removed by Hanning smoothing) but no broad feature became apparent up to a contrast of 10^5.

3. RESULTS

3.1. *HH 7–11*

This source lies in the NGC 1333 region at a distance of 350 pc (Herbig & Jones 1983). The molecular outflow mapped by Liseau, Sandell, & Knee (1988) consists of two partially overlapping lobes; the blue one extends southeast of SVS 13, the putative central object, and the red one, which is about twice as extended, northwest. SVS 13 is a highly variable source presently experiencing an outburst phase which started between 1988 December and 1990 September (Eislöffel et al. 1991). The apparent size of the red lobe is less than 4′, which is rather small for mapping with the Arecibo beam. Nevertheless we observed four different positions, as detailed in Table 1 and illustrated in Figure 2. The central one (C), coinciding with SVS 13, is the position already observed in Paper I. NW1 is displaced half a beam from the center and is situated within the red lobe near the CO column density maximum according to Figure 3*a* of Liseau et al. (1988). NW2 sits on the margin of the red lobe. We also spent some integration time on a southeast position (SE), that is located in the blue lobe, but, as customary in this sky area, the negative velocities are disturbed by unrelated clouds along the line of sight so that we chose to concentrate on the red-lobe points.

The resulting spectra for the three selected positions are illustrated in Figure 3. The lower noise of the C spectrum is due to the combination the present data with those of Paper I, so that the effective ON integration time for this spectrum climbs up to 450 minutes. The C profile is characterized by the presence of a clear wing profile; if we consider that the molecular cloud velocity (i.e., the probable systemic velocity of SVS 13) is $V_{LSR} = 8.2$ km s^{-1}, the wings extend symmetrically on both sides up to expansion velocities of about 170 km s^{-1} (± 15 km s^{-1}). While the blue side is somewhat disturbed by unrelated clouds, the red one is quite clean. Upon examination of the OFF spectra we estimate that the red wing is reliable down to $V_{LSR} \simeq 40$ km s^{-1}; the blue side instead is relatively clean only for $V_{LSR} \lesssim 65$ km s^{-1}, due both to unrelated clouds and to imperfect core cancellation. The NW1 spectrum is more noisy, but still the red wing is clearly visible. It appears that, while the (red) expansion velocity has declined to about 135 km s^{-1}, the flux density does not change appreciably. This is an indication that we are marginally resolving the neutral flow. This fact is confirmed upon examination of the blue wing which instead is substantially weaker, if detected at all. Finally the red wing is completely absent in the NW2 spectrum, which is the one mainly sampling regions outside the (red lobe) molecular flow. Since the procedure and the OFF positions used were the same for all the three spectra, the absence of winglike features in NW2 is the strongest argument for the reality and reliability of what is observed in C and NW1. As already noted in Paper I, within our noise figures and within the clean velocity ranges, the shape of the wings is triangular or anyway tapering toward high expansion velocities; this fact,

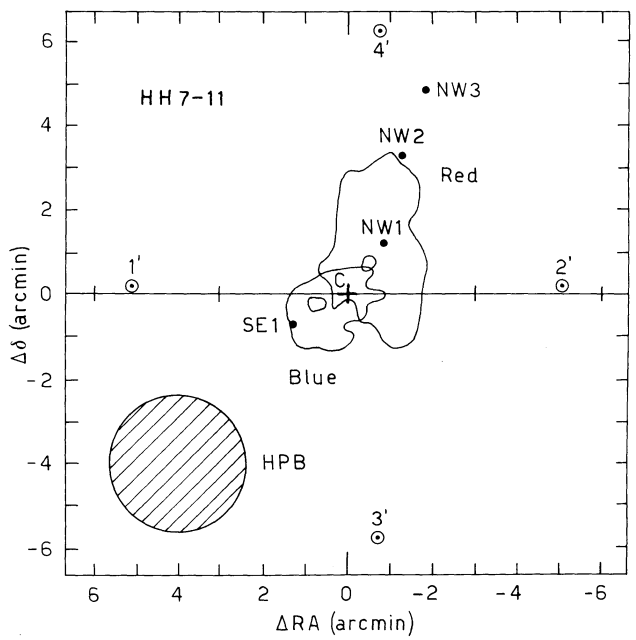

FIG. 2.—Schematic map of the CO outflow in HH 7–11 taken from Liseau, Sanders, & Knee (1988). The positions observed with the Arecibo beam, and reported in Table 1, are indicated. The central position (SVS 13), C in Table 1, is marked by a cross. The OFF's are also indicated, they are labeled 1′, 2′, 3′, and 4′. The axes are labelled by the displacement respect to the C position. The horizontal line passing through the center is the direction scanned by the frequency switching observations, the points observed are marked by tick marks.

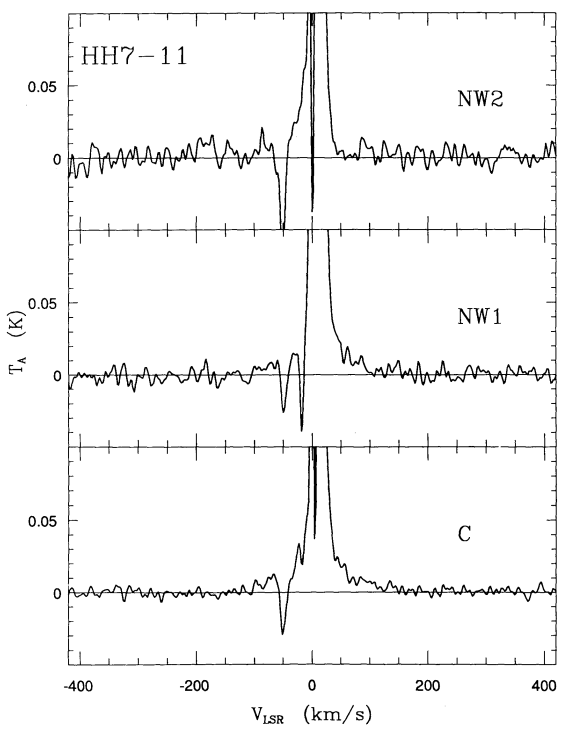

FIG. 3.—Spectra of HH 7–11 at the positions marked in Fig. 2. The high-velocity H I gas is present at positions C and NW1, but not at position NW2.

together with the lower maximum velocity observable in NW1, is indicative of a decelerating flow.

The neutral wind at intermediate velocities ($\lesssim 60$ km s^{-1}) was mapped by Rodríguez et al. (1990) who found it to be consistent with the low-velocity data in Paper I. The VLA spectra were not deep enough to detect the high-velocity H I. On the other side, they found the H I wind to have a bipolar morphology that coincides with the CO lobes. Our coarse mapping of the red lobe extends this finding to the high-velocity component of the wind, and it is consistent with extremely high-velocity CO mapped by Koo (1990).

3.2. *L1551*

This is a nearby object, part of the Taurus-Auriga complex, at a distance of 140 pc. The molecular outflow, as it appears from the CO map of Moriarty-Schieven & Snell (1988), is bipolar with the flow axis lying almost perpendicular to the line of sight with a position angle of $\sim 45°$. The blue south-western lobe extends for more than 15′; the red one appears to be less collimated and can be traced out to 12′. The apparent transverse width of the lobes is $\simeq 5'$. Since the line-of-sight velocity of the flow in this case is still large enough to discern the wind from the Galactic H I, the large extent of the lobes is ideal for mapping the wind. In addition, the central source of the outflow, IRS 5, lies at a Galactic latitude of $b_{II} = -20.0$, making the Galactic line core rather narrow and relatively weak ($T \simeq 50$ K). Unfortunately, as already mentioned, a system of intervening highly structured clouds renders the blue side of the spectra practically unusable for our purpose down to $V_{LSR} \lesssim -160$ km s^{-1}. Our study is therefore dedicated only to the redshifted flow. On this side of the spectra the core cancellation, as we could appreciate upon inspection of the OFF spectra, is quite good for $V_{LSR} > 45$ km s^{-1}. Four positions were observed: the central one (C) coincides with IRS 5; the other three are progressively displaced in north-east direction along the red outflow lobe as illustrated in Figure 4. IRS 5 was already observed in Paper I, who could only claim a marginal detection. The present data are summarized in Figure 5, where a red triangular wing extending to $V_{LSR} \simeq 150$ km s^{-1} grows in intensity from C to NE1, remains about unaltered and with little signs of deceleration in NE2, and finally disappears (almost) completely in NE3, that is, at the apparent border of the high-velocity CO flow. As for HH 7−11, the lower noise in the C spectrum was obtained by adding up the present observations with the data of Paper I.

3.3. *Other Sources*

In all of the following sources no high-velocity H I wings were detected. We briefly describe each of them separately here while H I mass upper limits are reported and discussed in § 4.3. In some of these sources the flow axis appears to be close to the plane of the sky (e.g., B335, RNO 43 S) and this might prevent the detection of high-velocity wings if the aperture of the flow cone is small. On the other hand, our best detection (L1551) is also in such unfavorable geometrical conditions.

RNO 43.—This region, which lies 480 pc away, has been searched for high-velocity molecular gas by Edwards & Snell (1984). Their map reveals a complex gas distribution which is interpreted as consisting of two distinct bipolar outflows, both with a projected extension of about 5′. The separation between the two outflow centers is about 4′. The southern outflow is roughly centered on the HH object RNO 43 itself, while no association with any known source has been found for the

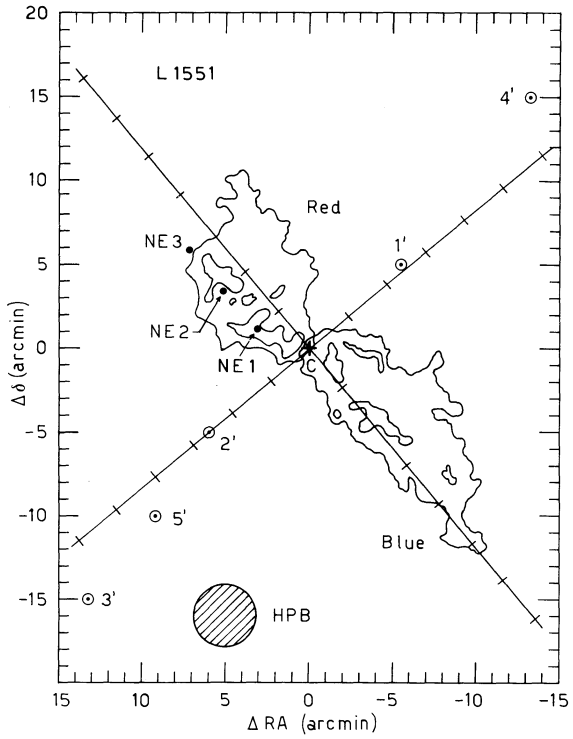

FIG. 4.—Schematic map of the CO outflow in L1551 taken from Moriarty-Schieven & Snell (1988). The positions observed with the Arecibo beam, and reported in Table 1, are indicated. The central position (IRS 5), C in Table 1, is marked by a cross. The OFF's are also indicated, they are labeled 1′, 2′, 3′, 4′, and 5′. The axes are labeled by the displacement respect to the C position. The two orthogonal lines passing through the center are the directions scanned by the frequency switching observations, the points observed are marked by tick marks.

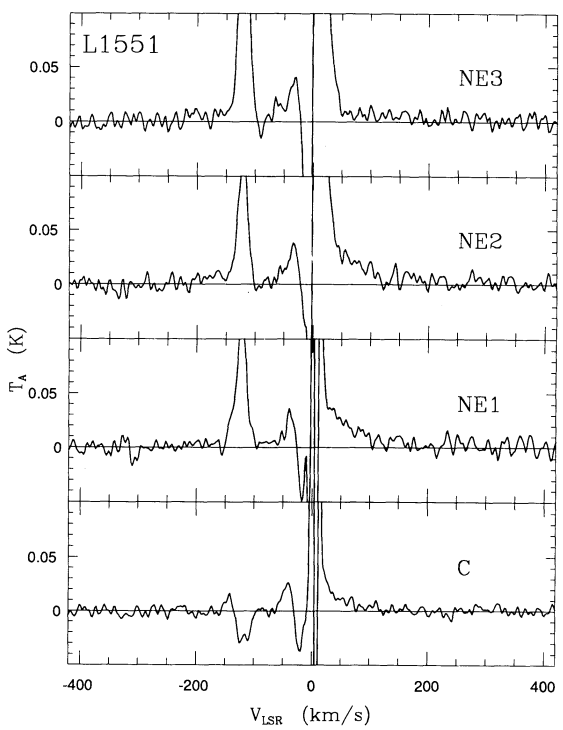

FIG. 5.—Spectra of L1551 at positions marked in Fig. 4. Note that the high-velocity H I gas is still present in position NE2, which coincides with the end of the CO outflow and it is not present at position NE3.

northern activity center. Notably, none of the outflows seems to be physically associated with the infrared objects in the area. We observed two positions: one centered on the northern (N) outflow, as it appears from the Edwards & Snell (1984) map, and the other one (S) centered on the southern one. In both cases the size of the Arecibo beam encompasses most of the outflow region. Despite a quite satisfactory core cancellation, especially in the S final spectrum, no wings were detected. In both spectra the rms noise is about 8 mK.

FU Ori.—This object is located into the southeastern extension of the B35 dark cloud at a distance of 500 pc. The CO map of Lada & Black (1976) shows that the star is located on the rim of the molecular cloud with a faint narrow CO feature that extends eastward from the source for about 13′. The position here observed coincides with the star. Several OFF pairs were chosen with different orientation respect to the molecular cloud morphology. The line core cancellation is satisfactory except for V_{LSR} between -37 and 47 km s^{-1}. The final rms noise outside of this range is 3.5 mK. No clear wing feature was detected and no mapping attempted.

R Mon.—The position observed is the one given by Levreault (1988b), and coincides with the star itself or the apex of the NGC 2261 nebula, at a distance of 800 pc. CO observations by Cantó et al. (1981) indicate a bipolar structure whose blue lobe is located within NGC 2261 itself and the red one is in the obscured region to the south of the star. The full extension of the outflow is about 3′, such that our beam should cover the whole high-velocity stream. The resulting spectrum is free from cancellation defects for $V_{LSR} > 71$ km s^{-1} on the red side. On the blue side, the comparison between the OFF's shows, despite the choice of different pairs, some residual baseline defect and we reject it. In the red range, the rms noise level is 5.2 mK.

NGC 2264.—A relatively faint CO outflow has been reported by Bally & Lada (1983) and Lada (1985). The outflow, which extends for about 4′, is monopolar, that is, only redshifted high-velocity molecular gas is observed. The only position observed here coincides with the surface density maximum in the outflow. Due to the low latitude ($l_{II} = 208.2$, $b_{II} = -0.6$), the Galactic line is wide and our clean range is limited to $-23 > V_{LSR} > 89$ km s^{-1}. Together with R Mon this is one of the relatively distant objects in our sample, 760 pc. The rms noise is 6.2 mK.

B335.—Within the B335 dark cloud, at a distance of 250 pc, a rather symmetric bipolar outflow has been mapped by Hirano et al. (1988). The outflow is east-west oriented, nicely centered on IRAS 19345+0727, it extends about 4′ on each side, and the outflow direction is approximately perpendicular to the line of sight. We did not point to the *IRAS* source but, given the extension of the flow, preferred to observe two positions approximately coincident with the centers of the two lobes: the east (E) position on the blue lobe and the west (W) on the red one. Unfortunately the considerable width of the Galactic line in this area ($l_{II} = 45.0$, $b_{II} = -6.6$) prevents a thorough cancellation for V_{LSR} between -44 and 122 km s^{-1} in both spectra and rather independently of the choice of OFF positions; the case appears therefore hopeless for the red lobe, but also in the blue one we find no hints of a wing. The final noise figure for both positions is 4.5 mK.

4. DISCUSSION

For an optically thin gas with a spin temperature much larger than the background temperature, the mass of H I is related to the observed antenna temperature T_A by

$$M_{\rm H\,I} = \mathscr{C}\left(\frac{d}{140\ \rm pc}\right)^2\left(\frac{\int T_A\,dv}{\rm K\ km\ s^{-1}}\right) M_\odot\ , \qquad (1)$$

where d is the distance to the source and $\mathscr{C}$ is a constant. For a point source ($\Omega < 1'.5$) and a telescope gain of the Arecibo telescope of $G = 7.5$ K Jy^{-1}, the constant is $\mathscr{C} = \mathscr{C}_p = 6.17 \times 10^{-4}$. For an extended source, assuming a Gaussian beam model with a FWHM = 3′.5 and a uniform hydrogen column density N_H within a radius $r < 2'$ and $N_H = 0$ for $r > 2'$, the constant is $\mathscr{C} = \mathscr{C}_{ex} = 9.36 \times 10^{-4}$.

4.1. *HH 7–11*

As mentioned in § 3, the spatial extent of the CO lobes in this source is too small to be fully resolved by the 21 cm Arecibo beam. Nonetheless, our coarse mapping is consistent with the idea that the neutral wind is partially resolved and decelerates away from the source. In Paper I a substantial entrainment of material from the walls of the lobes was invoked as the major cause of deceleration and of the resulting profile shape. In principle, the apparent deceleration could also be due to a secular variability of the wind characteristics induced by the variability, or better the evolution, of SVS 13. In any case, the spectra for HH 7–11 in Figure 3 show that the end of the H I flow (position NW2) coincides with the end of CO outflow, that is the neutral flow appears to be contained within the slowly expanding "high-velocity" CO lobe. The absence of high velocity H I in the NW2 spectrum suggests that either most of the region sampled by this beam has not been reached by the neutral flow, or the gas in the external regions has been decelerated to undetectable values. The position NW1 still shows high velocity H I, up to ~ 135 km s^{-1}.

The mass of atomic gas is given by $M_a = M_{\rm H\,I}/0.7$, where 0.7 corrects for a 30% He mass content. The momentum, in the velocity interval $[0, v_{max}]$, not corrected for inclination, is

$$P_a = \mathscr{K}\int_0^{v_{max}} T_a(v) v\,dv\ ,$$

where

$$\mathscr{K} = \mathscr{C}_{ex}(d/140\ \rm pc)^2/0.7\ .$$

The wind kinetic energy is $E_a = M_a \frac{1}{2} v^2$, where v is the real wind velocity. We take it equal to v_{max} because, given the substantial overlap of the two CO outflow lobes, we can assume that the observer lies within the cone of the flow. Also, the inclination angle with respect to the line of sight is $i \sim 22°$ (Herbig & Jones 1983). As noted before and discussed in Paper I, the line profiles are indicative of a decelerating wind but, since the source is only partially resolved, we do not know how much deceleration occurs inside each beam. Therefore, we choose to use the maximum velocity to calculate the energy at each position. Table 2 shows the computed values for the above quantities, together with the assumed maximum velocity v_{max}, at the different positions observed in the red lobe. To obtain these values, we have assumed that the source is resolved and that the line profiles have a triangular shape. In this case, the antenna temperature is given by $T_a(v) = m(v_{max} - v)$, with a slope $m = 1.5 \times 10^{-4}$ K km s^{-1} for position C and $m = 2.0 \times 10^{-4}$ K km s^{-1} for position NW1, both determined from $v > 40$ km s^{-1} (see § 3).

Liseau et al. (1988) found that the molecular mass in the red lobe of HH 7–11 is $M(\rm CO) > 2.0\ M_\odot$, but they point out that

TABLE 2

PARAMETERS OF THE ATOMIC WIND IN THE RED LOBE OF HH 7–11

Position	V_{max} (km s^{-1})	M_a ($M_\odot$)	P_a ($M_\odot$ km s^{-1})	E_a (ergs)
C	170	1.8×10^{-2}	1.0	5.2×10^{45}
NW1	135	1.5×10^{-2}	0.7	2.7×10^{45}

NOTES.—The mass and momentum of the atomic wind are corrected for a 30% abundance of helium. The momentum P_a is not corrected for inclination.

TABLE 3

PARAMETERS OF THE ATOMIC WIND IN THE RED LOBE OF L1551

Position	V_{max} (km s^{-1})	M_a ($M_\odot$)	P_a ($M_\odot$ km s^{-1})	E_a (ergs)
C (IRS 5)	100	1.5×10^{-3}	0.05	4.5×10^{44}
NE1	150	3.5×10^{-3}	0.18	2.4×10^{45}
NE2	150	3.5×10^{-3}	0.18	2.4×10^{45}

NOTES.—The mass and momentum of the atomic wind are corrected for a 30% abundance of helium. The momentum P_a is not corrected by inclination.

the mass could be smaller, since there are multiple sources in the region. The mean velocity of this flow is $\overline{v_{CO}} = 5$ km s^{-1}. For a momentum conserving wind, the momentum required to drive a molecular outflow with momentum P_{CO} is $P_w = (\overline{v_{CO}}/v_w)P_{CO}$. If one considers $v_w = v_{max}$, one would obtain the minimum required momentum to drive the CO outflow. If instead, as in Paper I, a mean velocity $v_w = 170/3 \sim 60$ km s^{-1} is considered (because the wind decelerates yielding a triangular profile) we derive a stronger constraint. The required momentum in this last case is $P_w \sim 0.94\ M_\odot$ km s^{-1}. Table 2 shows that there is enough momentum in the wind observed at position C. This value is a lower limit to the actual momentum in the whole wind because there is additional momentum in position NW1 but it is not possible, with the present spatial resolution, to correct for the overlap with position C. In any case, it is clear that the neutral wind found in HH 7–11 has enough momentum to drive the observed CO outflow.

The crossing time for a constant velocity wind in a cone with an inclination angle i with respect to the line of sight is given by $\tau_{cross} = (l_{max}/\sin i)/v$, where l_{max} is the projected size measured by the observer and v is the real wind velocity. If we assume that the wind has projected size comparable to the Arecibo beam $l_{max} = 0.35$ pc, the minimum crossing time is $\tau_{cross} \sim 2050$ yr, where a full velocity of 170 km s^{-1} was assumed. This implies a (maximum) mass-loss rate $\dot{M} = 8.8 \times 10^{-6}\ M_\odot$ yr^{-1} at position C and a wind kinetic luminosity $L_w = \frac{1}{2}\dot{M}v^2 = 20\ L_\odot$, which is 20% of the bolometric luminosity of SVS 13, $L_* \sim 100\ L_\odot$ (Cohen & Schwarz 1987).

It might be argued that the data by Herbig & Jones (1983) provide only a lower limit to the inclination i of the flow axis to the line of sight. In fact, the proper motions of the HH objects are thought to measure the pattern speed of the internal shocks, which can be only a fraction of the true flow velocity. If this is indeed the case, that is if the flow is not so close to the line of sight, our previous considerations regarding the momentum content remain virtually unchanged because they apply to the projected velocities of both the CO and H I flow. In contrast, the wind kinetic luminosity does change appreciably: if $i \simeq 45°$, instead of 22°, and the flow cone semi-aperture is $\alpha \simeq 20°$, such as in L1551, we estimate an $L_w = 80\ L_\odot$, which approaches the whole bolometric luminosity of SVS 13.

HH 7–11 is one of the few objects for which there are available sensitive observations of the extremely high-velocity (EHV) molecular flow (Paper I; Koo 1989; Masson, Mundy, & Keene 1990). The detected EHV CO appears to be confined to unresolved blobs (with 20″–30″ HPBW) in the area encompassed by our central beam. The fact that we see no evidence for peaks, or any spectral feature, at the velocities of the CO blobs is not surprising given the high beam dilution.

4.2. *L1551*

To derive the wind physical parameters from the line profiles shown in Figure 5, we take the line shape to be triangular with a slope $m = 2.3 \times 10^{-4}$ K km s^{-1} for all of the three spectra showing a red wing. Such slope is determined from velocities $v > 45$ km s^{-1} (see § 3). Table 3 shows the values of the maximum velocity v_{max}, the mass (M_a), the momentum not corrected for inclination (P_a), and kinetic energy (E_a) of the atomic high-velocity gas. To obtain the energy, we calculate the real velocity for a constant velocity wind with opening angle α and inclination angle i: $v = v_{max}/\cos(i - \alpha)$. We take $\alpha \sim 20°$ from the maps of Moriarty-Schieven & Snell (1988). The inclination angle is estimated to be $i \sim 75°$ from the space motion of HH29 (Snell & Schloerb 1985). With these parameters, the total real velocity corresponding to $v_{max} = 150$ km s^{-1} is $v = 260$ km s^{-1}. Note that the highest velocity of the H I gas in the profile, v_{max}, seems to be lower at the central position ($v_{max} = 100$ km s^{-1}). We argue that this happens because this spectrum has slightly lower signal to noise than the spectra of the other two positions, due to the fact that part of the material filling the beam is blueshifted.

The CO observations of the red lobe of L1551 by Moriarty-Schieven & Snell (1988) imply a swept-up molecular mass of $M_{CO} = 1.56\ M_\odot$ and a total momentum of the swept-up mass of $P_{CO} = 6.5\ M_\odot$ km s^{-1}. The momentum needed to drive this CO shell is $P_w = (\overline{v_{CO}}/v_{max})P_{CO} = 0.18\ M_\odot$ km s^{-1}, where we assumed a mean velocity of the CO $\overline{v_{CO}} = 4.2$ km s^{-1} and a constant velocity wind with $v_{max} = 150$ km s^{-1} (both line-of-sight velocities; uncorrected for inclination).

From the data of Table 3, we find a total momentum in the atomic wind (summing the three positions) of $P_w \sim 0.4\ M_\odot$ km s^{-1} which is twice as much as the required momentum. Given the uncertainties in the CO opacity, this is in very good agreement with the required momentum. There is also an indication that the wind is decelerating with distance from the source as in the case of HH 7–11 (see below). Then, $v_{max} = 150$ km s^{-1} would be an overestimate of the mean wind velocity.

The total projected length of the red lobe is $l_{max} = 1.1 \times 10^{18}$ cm (8.′75 at 140 pc). Given $i \sim 75°$, and $v = 260$ km s^{-1} as mentioned above, the crossing time across the whole lobe is $\tau_{cross} \sim 1400$ yr. Taking the total atomic mass in the lobe, this implies a wind mass-loss rate $\dot{M} = 6 \times 10^{-6}\ M_\odot$ yr, a massive wind as in the case of HH 7–11. The total wind kinetic luminosity is $L_w = 33\ L_\odot$. This wind luminosity exceeds the bolometric luminosity of IRS 5, $L_w > L_* = 26\ L_\odot$ (Levreault 1988a), but, as we will discuss below, this is an overestimate because the wind should be decelerating as indicated by the modeling of the line profiles (see discussion below). In any case, this value is in better agreement with the results of Clark et al. (1986) who found the diffuse far infrared luminosity in L1551

(which would correspond to the mechanical luminosity deposited by the wind in the surrounding medium) to be $L_{FIR} > 19\ L_\odot$, rather than with those of Edwards et al. (1986) who found only 6 $L_\odot$.

As shown in Figure 5, the high-velocity H I extends up to the end of the CO lobe. Outside (position NE3), the H I spectrum shows no high velocity gas. This means that the momentum and energy of the material that reaches the end of the lobe, are deposited, possibly through a shock, into the ambient cloud. It is interesting to note that OH in absorption is observed at the tip of the red lobe. Detailed non–LTE modeling of the OH excitation state shows that this can be explained as the result of compression suffered in a shocked layer (Ruiz 1991). Near-IR observations of this region might reveal the presence of shocked molecular gas.

In Figure 6 we present the line profiles of an optically thin atomic wind moving at constant velocity $v = 300$ km s^{-1}, in a cone with opening angle $\alpha = 20°$ and inclination angle $i = 75°$. It is clear that a constant velocity wind does not reproduce the observed line profiles steepening towards low velocities ("triangular"). Motivated by this result, we have modeled the line profiles of an optically thin atomic wind that decelerates as mass is entrained along the walls of the cone (see also Paper I). These models are characterized by a velocity at the base v_0, a mass-loss rate $\dot{M}$ and a maximum lobe size r_{max}. Material is entrained from the walls only up to an entrainment angle θ_{ent}, and the material is decelerated radially to half of v_0 at a radius r_{ent} and $\theta = \alpha$. A more detailed description of the modeling is given in the Appendix. Here we present the results for only one of these decelerating wind models. Figure 7 which shows the line profiles, corresponding to the four positions observed at Arecibo, for a wind model with a velocity at the base $v_0 = 300$ km s^{-1}, a mass loss rate $\dot{M} = 2.4 \times 10^{-6}\ M_\odot$ yr^{-1}, a lobe size $r_{max} = 10'$, a deceleration radius $r_{ent} = 1'.4$, and an angle of entrainment $\theta_{ent} = 12°$. The model also assumes that the material of the molecular cloud, which is being entrained, has a radial density distribution $\rho_c = \rho_0(r/r_0)^{-\gamma}$, with $\gamma = 1.5$. The uppermost profile corresponds to the end of the lobe. Due to the deceleration within the entrainment layer, we are able to reproduce the line profiles by using a mass-loss rate which is a factor of 3 smaller than that obtained by assuming a constant velocity wind. In particular, in this model, the wind has been decelerated to $0.27v_0$ at r_{max} (eq. [A3]). The kinetic luminosity of the model is $L_w = 17\ L_\odot$, half of the luminosity previously estimated for a constant velocity wind, and less than the bolometric luminosity of the IRS 5 source.

Notably, although it is not possible to constrain observationally all the parameters involved in the modeling, the line profiles are not easy to reproduce with arbitrary choices of the deceleration parameter and of the entrainment angle. In fact, the model we presented here provides the most reasonable fit to the data. In particular, it is interesting to mention that the profiles are not consistent with either a constant velocity wind,

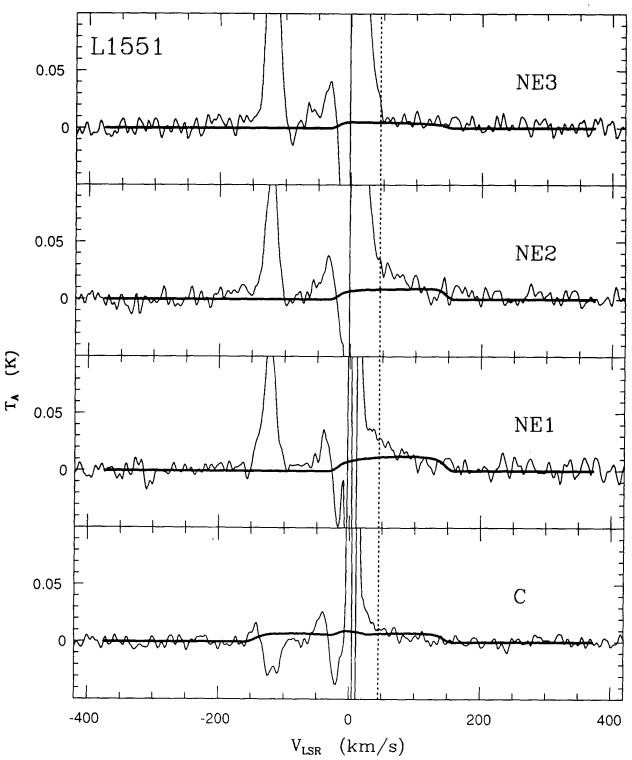

FIG. 6.—H I line profiles (*thick line*) produced by an optically thin constant velocity wind, with $v_w = 260$ km s^{-1} and $\dot{M} = 2.4 \times 10^{-6}\ M_\odot$ yr^{-1}. The wind blows in a cone with opening angle $\alpha = 20°$ and inclination angle of the axis with respect to the line of sight $i = 75°$. The NE3 position approximately coincides with the end of the cone in the wind model, which has a projected extension of 10′. Clearly they do not fit the triangular shape of the observed profiles (*thin line*).

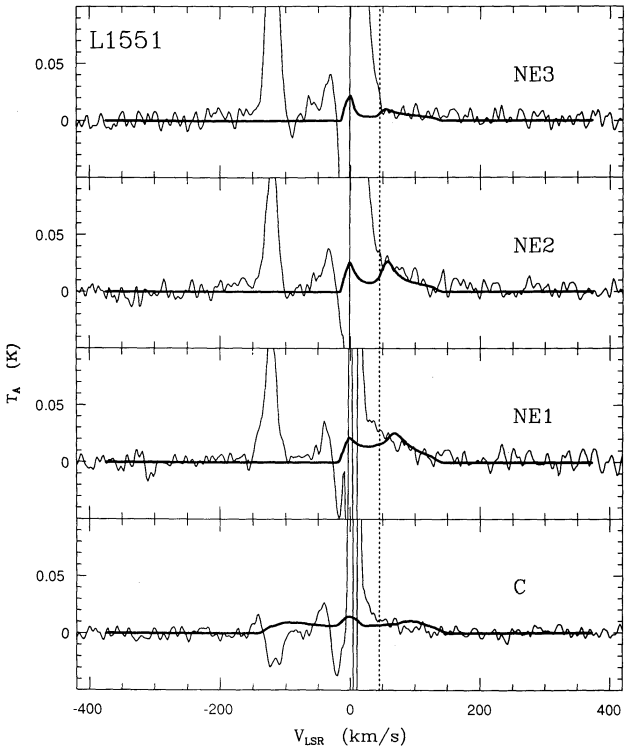

FIG. 7.—H I line profiles (*thick line*) produced by an optically thin decelerating wind, with a velocity at the base $v_0 = 300$ km s^{-1} and $\dot{M} = 2.4 \times 10^{-6}\ M_\odot$ yr^{-1}. The wind blows in a cone with opening angle $\alpha = 20°$ and inclination of the axis with respect to the line of sight $i = 75°$. The wind decelerates because material is entrained from the walls of the cone down to an entrainment angle $\theta_{ent} = 12°$ such that it is decelerated radially to half of v_0 at a projected radius $r_{ent} = 1'.4$ (see Appendix). The NE3 position approximately coincides with the end of the cone in the wind model, which has a projected extension of 10′. This model provides the best fit to the observed H I profiles (*thin line*).

TABLE 4

ATOMIC MASS UPPER LIMITS IN THE UNDETECTED OBJECTS

Position	Distance (pc)	Noise (mK)	Δv (km s^{-1})	Atomic Mass (10^{-2} $M_\odot$)	Notes
RNO 43 N	480	7.5	200	2.4	Full N outflow
RNO 43 S	480	8.5	200	2.7	Full S outflow
FU Ori	500	3.5	200	1.2	No CO outflow
R Mon	800	5.2	100	2.3	Red lobe only[a]
NGC 2264	760	6.2	100	2.5	Red lobe only
B 335 W	250	5.0	100	(0.2)[b]	Red lobe
B 335 E	250	4.2	100	0.2	Blue lobe

[a] Blue side rejected because of baseline defects.
[b] Incomplete concellation of the line core.

or a wind that decelerates only in the radial direction (Paper I), or a wind which decelerates only in the θ direction (Edwards et al. 1987).

4.3. *Other Sources*

In order to obtain a limit for the wind mass for the objects where no high-velocity H I was detected, we assumed a triangular profile (for the red and blue range of velocities) with half-power intensity $T_A = 2\sigma_{\rm rms}$, where $\sigma_{\rm rms}$ is the rms noise of the spectrum, and base $\Delta v = 2v_{\rm max}$ (if both red- and blueshifted gas is considered) or $\Delta v = v_{\rm max}$ (if only one lobe is considered). Using equation (1), assuming the sources are resolved, the upper limit to the mass[2] of atomic gas is

$$M_{\rm lim} = 1.2 \times 10^{-2}\left(\frac{d}{500\ {\rm pc}}\right)^2 \times \left(\frac{\sigma_{\rm rms}}{3.5 \times 10^{-3}\ {\rm K}}\right)\left(\frac{\Delta v}{200\ {\rm km\ s^{-1}}}\right) M_\odot\ .$$

The distance d, rms noise, assumed Δv, and mass limit for RNO 43, FU Ori, R Mon, NGC 2264, and B335 are shown in Table 4. In particular, in the case of FU Orionis, the $M_{\rm lim}$ can be used to set a limit on the mass loss rate associated to the outburst that initiated in 1937 (e.g., Herbig 1989). Assuming that the wind is neutral,

$$\dot{M}_{\rm outburst} < \frac{M_{\rm lim}}{53\ {\rm yr}} = 2.1 \times 10^{-4}\ M_\odot\ {\rm yr}^{-1}\ .$$

In this equation, we neglected the mass of the wind in the quiescent phase because, for typical T Tauri wind parameteters ($\dot{M} \sim 10^{-8}$ $M_\odot$ yr $^{-1}$, $v_w \sim 200$ km s^{-1}), the amount of H I still within the Arecibo beam, i.e., in a wind crossing time $\tau_{\rm qui} \sim 2200$ yr, is only $M_{\rm qui} \sim 2.2 \times 10^{-5}$ $M_\odot$, which is three orders of magnitude smaller than $M_{\rm lim}$. This is not a stringent limit because current models of FU Ori require $\dot{M} \sim 10^{-5}$ $M_\odot$ yr^{-1} (e.g., Crosswell, Harmann, & Avrett 1987; Hartmann, Kenyon, & Hartigan 1992).

The upper limits on the mass for the other sources are also not stringent since the momentum of the atomic wind associated with the upper limit on the mass, $P_a = M_{\rm lim} v_{\rm max}/3$, would be greater than that required to drive the observed CO outflows. Apart from B335 all the other sources would require mass limits lower by a factor of 10, on average, than the present ones. In the case of B335 our limit would already be significant but if the flow inclination is really as low, $i \simeq 10°$, as suggested by Hirano et al. (1988), then the emission would be limited to (absolute velocities) lower than 50 km s^{-1}, and therefore, buried within the line core.

[2] Corrected by a 30% abundance by mass of He.

5. SUMMARY

We have mapped the high-velocity neutral wind in HH 7–11. We find that the maximum velocity declines to $\sim$135 km s^{-1} in the NW1 position displaced half a beam from the center. This finding is consistent with the idea that the neutral wind is partially resolved and decelerates away from the source SVS 13, as has been proposed, on the basis of the line profiles, in Paper I.

We present a definite detection of the massive neutral wind in L1551. The extent of the outflow area in this case is well resolved by the Arecibo beam and we have mapped the high-velocity gas along the redshifted CO lobe.

The H I observations of HH 7–11 and L1551 support the picture in which the CO outflow is driven by a fast neutral stellar wind that conserves momentum and drives the observed high-velocity molecular outflows. From the observations, the maximum mass-loss rate (assuming a constant velocity wind) and maximum velocity for HH 7–11 are $\dot{M} = 8.8 \times 10^{-6}$ $M_\odot$ yr^{-1} and $v \sim 170$ km s^{-1}. For L1551 they are $\dot{M} = 6 \times 10^{-6}$ $M_\odot$ yr^{-1} and $v \sim 260$ km s^{-1}. In both cases, the wind has enough momentum to drive the observed high-velocity CO outflows.

Since the high-velocity H I in L1551 extends up to the end of the CO lobe, a substantial fraction of the momentum and energy of the wind must be deposited, possibly through a shock, into the ambient cloud. The presence of such a shock is also suggested by the OH in absorption observed at the tip of the red lobe, which seems to be the result of non–LTE effects in a compressed gas (Ruiz 1991).

In the case of L1551, we find high-velocity H I all along the lobe with the characteristic triangular profiles indicative of deceleration. We presented a simple model which parameterizes the process of mass entrainment in the atomic wind. This model reproduces the intensity and shape of the observed line profiles. The entrainment of molecular material decelerates the wind from an initial velocity $v_0 = 300$ km s^{-1} to a third of this value at the end of the lobe. The mass-loss rate associated with the model is $\dot{M} = 2.4 \times 10^{-6}$ $M_\odot$ yr^{-1}, 3 times smaller than that estimated assuming a constant velocity wind.

For the undetected objects (RNO 43, R Mon, NGC 2264, B335), the upper limits on the atomic high-velocity gas are not stringent. Therefore, even if no high velocity H I was detected,

the observed molecular outflows could still be driven by massive neutral winds. Finally, the upper limit on the atomic mass in the case of FU Ori, sets a limit on the mass loss rate during the active phase which initiated with the outburst in 1937. Again, this is not a stringent limit because it is still an order of magnitude larger than the mass-loss rates required by current models of FU Ori objects.

We thank Willem Baan and the staff of the Arecibo Observatory for their keen assistance during the observations. We thank Jorge Cantó, Loris Magnani, Felix Mirabel, Francesco Palla, Abraham Ruíz, and Frank Shu for useful comments and discussions. C. G. would like to gratefully acknowledge the exquisite hospitality of Carmen and Abraham Ruíz, and the generous support of the Instituto de Astronomia UNAM.

APPENDIX

Consider the situation depicted in Figure 8. The wind flows in a cone with opening angle α; due to mass entrainment from the walls of the cone, there is a transverse flux of mass $\sigma(r, \theta)$ (g s^{-1} cm^2) at distance r from the center of the outflow, at an angle θ from the axis.

Assuming azimuthal symmetry, the equation of continuity in spherical coordinates is

$$\frac{1}{r^2}\frac{\partial(r^2\rho v)}{\partial r} = \frac{1}{r\sin\theta}\frac{\partial(\sigma\sin\theta)}{\partial\theta}, \tag{A1}$$

where ρ is the total density (wind plus entrained material) and v is the radial velocity of the flow. This is the equation of continuity for a flow with a transverse velocity component $v_\theta = \sigma/\rho$.

Assuming that the $v_\theta \ll v$, momentum is conserved in the radial direction. Then,

$$\rho r^2 v^2 = \dot{A}_1 v_0, \tag{A2}$$

where $\dot{A}_1$ is the mass-loss rate per steradian (g s^{-1} sr^{-1}), and v_0 is the wind velocity before entrainment.

Using equations (A1) and (A2), the velocity of the gas is

$$v(r, \theta) = \frac{v_0}{1 + \epsilon(r, \theta)}, \tag{A3}$$

where we define an entrainment function

$$\epsilon(r, \theta) \equiv \frac{1}{\dot{A}_1}\int_{r_i}^{r}\frac{1}{\sin\theta}\frac{\partial(\sigma\sin\theta)}{\partial\theta}\, r\, dr, \tag{A4}$$

where r_i is the radius where entrainment begins. Since this simple model is just a parameterization of the process of mass entrainment, we choose to give a reasonable function for ϵ in the following way. The flux of entrained material at the walls of the cone is given by $\sigma = e\rho_c(r)c_c$ where ρ_c is the density of the molecular cloud, c_c is the sound speed, and e is an efficiency factor (Cantó & Raga 1991). If the radial density profile of the molecular cloud is a function $\rho_c = \rho_0(r/r_0)^{-\gamma}$, and the cloud is isothermal, we take

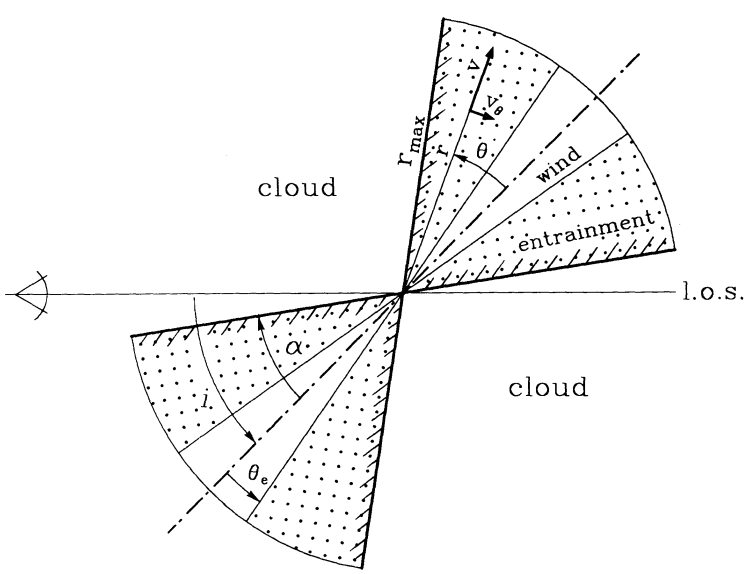

FIG. 8.—Schematic picture of the H I flow model described in the Appendix. The atomic wind flows freely in the inner part of the cone, while it is decelerated in the (*dotted*) outer part by entrainment of cloud material.

$\sigma(r, \theta) = \sigma_0(r/r_0)^{-\gamma} f(\theta)$, where $f(\theta)$ determines the mass flux in the θ direction. Because of the decrease in the molecular cloud density, less mass is entrained as the flow moves further into the cloud. With this motivation, we write equation (A4) as

$$\epsilon(r, \theta) = \left(\frac{r}{r_{\rm ent}}\right)^{2-\gamma} F(\theta) , \tag{A5}$$

where $F(\theta) = [\partial \sin \theta f(\theta)/\partial\theta]/\sin(\theta)/(2-\gamma)$, and where the magnitude of the entrainment radius $r_{\rm ent}$ determines the efficiency of the entrainment process in the radial direction. For simplicity, we take $F(\theta) = (\theta - \theta_{\rm ent})/(\alpha - \theta_{\rm ent})$, such that the entrained material arrives only up to the entrainment angle $\theta_{\rm ent}$. According to equation (A3), the velocity profile varies smoothly as a function of θ from v_0 at $\theta = \theta_{\rm ent}$ to a minimum velocity $v(r, \alpha) = v_0/[1 + (r/r_{\rm ent})^{2-\gamma}]$ at the opening angle α. For a given model we choose the wind initial velocity v_0, the radius $r_{\rm ent}$ and angle of entrainment $\theta_{\rm ent}$. Finally, to mimic the morphology of L1551 (Fig. 4), we assign a finite radial size to the cone $r_{\rm max}$.

In order to obtain the H I profiles, two additional assumptions were made: (1) the gas is optically thin, and (2) the mass of atomic hydrogen is conserved. Given the high velocity and low column density involved, the first assumption is basically correct. The second assumption will be violated if substantial dissociation of the molecular gas occurs in the entrainment process.

Finally, we want to point out that this model does not describe the region that would actually be observed as the CO lobe. The wind considered here decelerates across the entrainment region to velocities that are a substantial fraction of its original velocity, still much higher than the velocities of the CO outflows. This means that there is still a region outside the cone of the wind ($\theta = \alpha$) where a viscous coupling with the molecular gas has to occur. An extensive discussion about the line profiles and the energetics of mass entraining winds will be presented elsewhere (Giovanardi & Lizano 1992).

REFERENCES

Appenzeller, I., & Mundt, R. 1990, A&A, Rev., 1, 291
Bally, J., & Lada, C. J. 1983, ApJ, 265, 824
Bally, J., & Stark, A. 1983, ApJ, 266, L61
Cabrit, S., & Bertout, C. 1990, ApJ, 348, 530
Cantó, J., & Raga, A. 1991, ApJ, 372, 646
Cantó, J., Rodríguez, L. F., Barral, J. F., & Carral, P. 1983, ApJ, 244, 102
Clark, F. O., Laurejis, R. J., Chlewicki, G., Zhang, C. J., van Oosterom, W., & Kester, D. 1986, A&A, 168, L1
Cohen, M., & Schwarz, R. D. 1987, ApJ, 316, 311
Croswell, K., Hartmann, L., & Avrett, E. H. 1987, ApJ, 312, 227
De Campli, W. M. 1981, ApJ, 244, 124
Dyson, J. E. 1984, Ap&SS, 106, 181
Edwards, S., Cabrit, S., Strom, S. E., Heyer, I., Strom, K. M., & Anderson, E. 1987, ApJ, 321, 473
Edwards, S., Strom, S. E., Snell, R. L., Jarret, T. H., Beichman, C. A., & Strom, K. M. 1986, ApJ, 307, L65
Edwards, S., & Snell, R. L. 1984, ApJ, 281, 237
Eislöffel, J., Günther, E., Hessman, F. V., Mundt, R., Poetzel, R., Carr, J. S., Beckwith, S., & Ray, T. P. 1991, ApJ, 383, L19
Evans II, N. J., Levreault, R. M., Beckwith, S., & Skrutskie, M. ApJ, 320, 364
Giovanardi, C., Gennari, S., Natta, A., & Stanga, R. 1990, ApJ, 367, 173
Giovanardi, C., & Lizano, S. 1992, in preparation
Hartmann, L., Kenyon, S. J., & Hartigan, P. 1992, in Protostars and Planets III, ed. E. H. Levy & J. Lunine (Tucson: Univ. Arizona Press), in press
Herbig, G. H. 1989, in ESO Conference and Workshop Proceedings 33, Low Mass Star Formation and Pre–Main-Sequence Objects, ed. B. Reipurth (Munich: ESO), 233
Herbig, G. H., & Jones, B. F. 1983, AJ, 88, 1040
Hirano, N., Kameya, O., Nakayama, M., & Takakubo, K. 1988, ApJ, 327, L69
Koo, B.-C. 1989, ApJ, 337, 318
———. 1990, ApJ, 361, 145
Kwok, S., & Volk, K. 1985, ApJ, 327, L69
Lada, C. J. 1985, ARA&A, 23, 267
Lada, C. J., & Black, J. H. 1976, ApJ, 203, L75
Lizano, S., Heiles, C., Rodríguez, L. F., Koo, B.-C., Shu, F., Hasegawa, T., Hayashi, S., & Mirabel, I. F. 1988, ApJ, 328, 763 (Paper I)
Levreault, R. M. 1988a, ApJ, 330, 897
———. 1988b, ApJS, 67, 283
Liseau, R., Sandell, G., & Knee, L. B. G. 1988, A&A, 192, 153
Masson, C. R., Mundy, L. G., & Keene, J. 1990, ApJ, 357, L25
Moriarty-Schieven, G. H., & Snell, R. L. 1988, ApJ, 332, 364
Mundt, R., Brugel, E. W., & Bührke, T. 1987, ApJ, 319, 275
Natta, A., & Giovanardi, C. 1990, ApJ, 356, 646
Natta, A., Giovanardi, C., & Palla, F. 1988, ApJ, 332, 921
Natta, A., Giovanardi, C., Palla, F., & Evans II, N. J. 1988, ApJ, 327, 818
Pudritz, R. E., & Norman, C. A. 1983, ApJ, 274, 677
Raga, A. C. 1989, in ESO Conference and Workshop Proceedings 33, Low Mass Star Formation and pre–Main-Sequence Objects, ed. B. Reipurth (Munich: ESO), 281
Rodríguez, L. F., & Cantó, J. 1983, Rev. Mexicana Astron Af., 8, 163
Rodríguez, L. F., Lizano, S., Cantó, J., Escalante, V., & Mirabel, I. F. 1990, ApJ, 365, 261
Ruiz, A. 1991, Ph.D. thesis, Universidad Nacional Autonoma de Mexico
Ruiz, A., Alonso, J. L., & Mirabel, I. F. 1991, preprint
Russell, A. P. G., Hills, R. E., Padman, R., & Bally, J. 1991, preprint
Shibata, K., & Uchida, Y. 1985, PASJ, 37, 31
Snell, R. L., Bally, J., Strom, S. E., & Strom, K. M. 1985, ApJ, 290, 587
Snell, R. L., & Schloerb, F. P. 1985, ApJ, 295, 490
Shu, F., Lizano, S., Ruden, S. P., & Najita, J. 1987, ApJ, 328, L19
Shu, F., Ruden, S. P., Lada, C. J., & Lizano, S. 1991, ApJ, 370, L31
Strom, K. M., Strom, S. E., Wolf, S. C., Morgan, J., & Wenz, M. 1986, ApJS, 62, 39
Terebey, S., Beichman, C. A., Gautier, T. N., Hester, J. J., Myers, P. C., & Vogel, S. N. 1991, in IAU Symp. 147, Fragmentation of Molecular Clouds and Star Formation, ed. E. Falgarone, F. Boulanger, & G. Duvert (Dordrecht: Kluwer), 345